Journal of Alloys and Compounds 505 (2010) 459–466

Contents lists available at ScienceDirect

Journal of Alloys and Compounds

journal homepage: www.elsevier.com/locate/jallcom

On the fabricability of a composite material containing the FCC matrix with embedded ductile B2 intermetallics

Mehdi Hosseinifar*, Dmitri V. Malakhov

Department of Materials Science and Engineering, McMaster University, 1280 Main St. W., Hamilton, ON, L8P4L7, Canada

ARTICLE INFO

Article history:
Received 8 February 2010
Received in revised form 16 April 2010
Accepted 24 April 2010
Available online 19 June 2010

Keywords:
Rare-earth alloys and compounds
Al-La-Mg system
Calorimetry
Thermodynamic modeling

ABSTRACT

An imaginary composite material containing a ductile Al-rich FCC matrix with embedded particles of ductile RMg intermetallics (R is a rare-earth metal) may possess high strength and formability thus making it suitable as a replacement for steel in automotive applications. Although different fabrications routes can be explored, a direct-chill casting is likely least expensive of them. A crucial question is whether it is possible to find such a composition of the ternary Al–R–Mg melt whose solidification would result in the desired Al/RMg structure. In order to answer the question, a thermodynamic model of the Al–La–Mg system was built using the CALPHAD method. The model, whose validity was demonstrated by calorimetric experiments, was then used to prove that the FCC + LaMg composite material could not be produced *via* casting. Similar properties of rare-earth metals suggest that the conclusion based on the analysis of the particular Al–La–Mg case, will likely remain valid for other rare-earth elements.

1. Introduction

In 2003, a family of ductile intermetallics was discovered by Gschneidner et al. [1]. This family encompasses binary stoichiometric compounds RM, where R is a rare-earth metal, and M is a transitional metal or a metal belonging to a main group. These intermetallic compounds have the CsCl (B2) crystal structure. While a great deal of attention was paid to individual RM phases [2–7], they were never considered as constituents enhancing such mechanical properties as formability and strength of alloys, in general, and Al alloys, in particular. However, it is known that an exceptionally high strength is achievable in certain materials made of two deformable phases when they undergo a severe deformation [8]. For example, a tensile strength exceeding 1.4 GPa was attained in a heavily deformed Cu–Fe alloy [9] and a Cu–Nb composite [10].

It is interesting to find whether such a high strength can be achieved in a material, in which ductile RM particles and a surrounding ductile Al-rich FCC matrix are co-deformed. Such a material could serve as a substitute of steel for automotive body panels. But before the material is tested, it has to be fabricated. The first complication is that none of numerous binary rare-earth aluminides is a member of the ductile intermetallics family [1]. Fortunately, magnesium, which is frequently utilized in wrought aluminum alloys, forms RM compounds. It can be anticipated that Mg concentration sufficient for triggering the formation of the RM phase would be much higher than that in 5xxx and 6xxx series of Al alloys, but this does not necessarily constitute a disadvantage due to a low density of magnesium and relentless efforts to reduce the weight of automotive parts. With respect to making a choice among the rare-earth metals, it seems reasonable to give preference to lanthanum as one of the least expensive of them. These arguments explain why the Al–Mg–La system is focused upon.

From the economic viewpoint, casting will be the most inexpensive way to fabricate an Al/RM composite, but a crucial question is whether it is possible to select such a composition of the ternary Al–Mg–La melt that its solidification will result in a desirable two-phase[1] microstructure. In order to answer this question, one has to either launch a laborious experimental investigation trying various compositions or rely upon computational thermodynamics. The latter approach does not necessitate a mass production of numerous solidification paths; information on the liquidus surface and regions of primary solidification may be sufficient to arrive at a definite conclusion. The calculations cannot be trusted if they are not based on a trustworthy thermodynamic description of the Al–Mg–La system, *i.e.*, on reliable models of all phases in this system. Building such a description using the CALPHAD technique [11] was one of the objectives of this work.

* Corresponding author. Tel.: +1 905 525 9140x23484; fax: +1 905 528 9295.
E-mail addresses: hossem@mcmaster.ca (M. Hosseinifar), malakhov@mcmaster.ca (D.V. Malakhov).

[1] Although the solidification of a ternary melt seldom results in a solid substance containing only two phases, the term "two-phase" is applied for brevity to a material in which FCC and RM dominate while fractions of other phases are relatively small.

0925-8388/$ – see front matter © 2010 Elsevier B.V. All rights reserved.
doi:10.1016/j.jallcom.2010.04.254

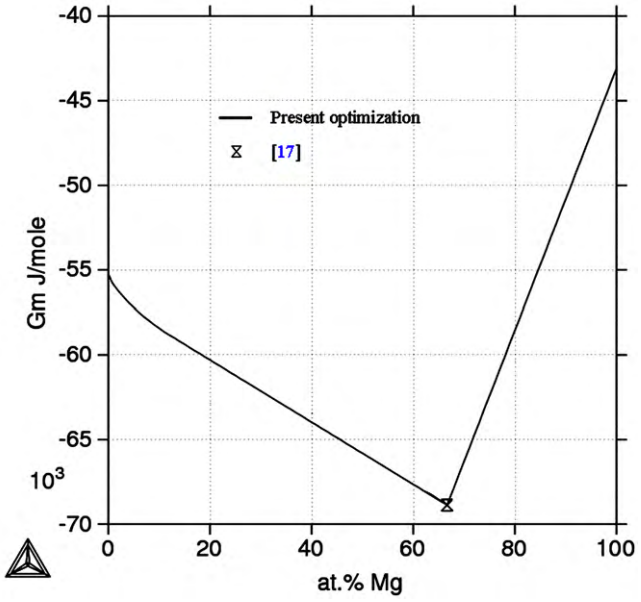

Fig. 1. The molar Gibbs energy of Mg_2La [17] and Laves_C15 [this work] at 1025 K.

2. Thermodynamics of the binary systems

An excellent thermodynamic description of the Al–Mg system [12] is trusted and used without alterations. It is worth mentioning that although a binary Laves_C15 phase Al_2Mg does not exist, its thermodynamic properties were evaluated by Saunders [13] who used a two-sublattice model $(\mathbf{Al},Mg)_2(Al,\mathbf{Mg})_1$ for that purpose (major constituents are bolded).

Although the Al–La system was optimized in 2000 [14] and 2001 [15], it was shortly reassessed by Zhou and Napolitano [16]. In this work, preference is given to [16], because it provides a much better agreement between calculated thermodynamic properties and the phase diagram with their experimental counterparts. Also, a three-species association model chosen by Zhou and Napolitano for describing thermodynamics of the liquid phase is more realistic than the Redlich–Kister formalism utilized by Cacciamani and Ferro. Physically feasible thermodynamic models of the phases constructed in [16] are trusted and employed without modifications. In particular, a two-sublattice model $(\mathbf{Al},La)_2(Al,\mathbf{La})_1$ used in that work to describe the Laves_C15 phase Al_2La along with the Gibbs energies of corresponding four end-members are accepted.

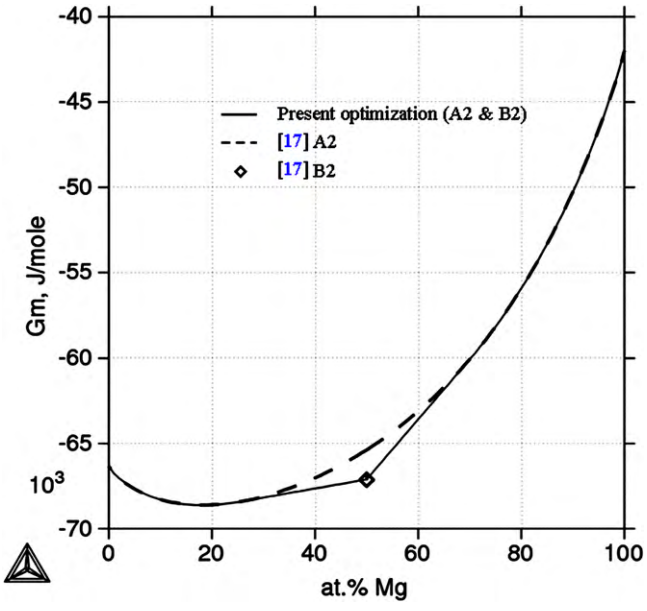

Fig. 2. The molar Gibbs energies BCC_A2 and BCC_B2 [17] and BCC_B2 [this work] at 950 K.

The La–Mg system was optimized by Guo and Du [17]. The Laves_C15 phase $LaMg_2$ was treated as a stoichiometric compound. Formally, the sublattice model of this phase can be written as $(Mg)_2(La)_1$, but in contrast to the models adopted for the Al_2Mg and Al_2La phases, Mg and La cannot reside in both sublattices. Let us recall that if it is intended to describe the thermodynamic properties of the Laves_C15 phase in the Al–Mg–La system, then according to the recommendations formulated by Ansara et al. [18], a crystallographically sound model would be $(Al,La,Mg)_2(Al,La,Mg)_1$. Since for the binary La–Mg case the model yields $(La,\mathbf{Mg})_2(\mathbf{La},Mg)_1$, $LaMg_2$ should formally be treated not as a daltonide but as a berthollide even though its homogeneity region is very narrow. Consequently, the thermodynamic model of this phase suggested by Guo and Du [17] has to be modified. It should be accentuated that the temperature dependence of the Gibbs energy of formation of $LaMg_2$ borrowed from their work forms a solid foundation for such an amendment.

In [17], LaMg, which, as one remembers, is one of ductile RM intermetallics, was handled as a routine stoichiometric compound. However, it is crystallographically justifiable to treat this B2 phase as an ordered BCC_A2 lattice. Although aluminum does not form B2 phases (AlLa has an AlCe oC16 crystal structure), it dissolves in LaMg. These two circumstances point to $(Al,La,Mg)_1(Al,La,Mg)_1(Va)_6$ as a suitable model for the ordered ternary B2 phase; an absence of interstitials justifies $(Al,La,Mg)_1(Al,La,Mg)_1$ as its abbreviated format. In the binary La–Mg case, it becomes $(La,Mg)_1(La,Mg)_1$. The Gibbs energy of formation of LaMg suggested in [17] is not ignored; it is retained and interpreted as a known Gibbs energy of formation of one of the end-members.

2.1. A partial optimization of the La–Mg system

Although the arguments presented above call for a reassessment of the La–Mg system, a full-fledged optimization is hardly warranted. Let us recall that the thermodynamic description of this system constructed by Guo and Du [17] provides an excellent agreement between the calculated and experimentally measure quantities, and that the thermodynamic models of only two phases, LaMg and $LaMg_2$, must be refined in order to provide their consistencies with the ternary Laves_C15 and B2 phases. It will be much easier to achieve this limited goal *via* a partial optimization. Such an approach is not alien to the computational thermodynamics community; it was practiced before. An instructive example can be found in [12] where the Gibbs energies of the liquid phase and terminal solid solution in the Al–Mg system were inherited without changes from [13] while the thermodynamic descriptions of intermediate intermetallics were re-evaluated. Another illustration is provided by [19], in which Dupin and Ansara investigated consequences which a revision of a sublattice model of the B2 phase in the Al–Ni and Ti–Ni led to.

In order to construct the thermodynamic models of the binary Laves_C15 and B2 phases in the La–Mg system, it was decided to rely upon information on invariant equilibria those phases participated in. Analytical expressions for the Gibbs energies of end-members and interaction parameters determined for the new models with the aid of PARROT [20] are given in Table 1. Since the constraints $G^0_{i:j} = G^0_{j:i}$ and ${}^0L_{*:i,j} = {}^0L_{j,i:*}$ (asterisk indicates i or j) are imposed by the crystallographic symmetry of the B2 phase, it is not surprising to see identical expressions for different Gibbs energies and inter-

Table 1
Thermodynamic characteristics of the Laves_C15, BCC_B2 and τ phases.

Parameter	Reference
Phase: Laves_C15, Sublattice model: $(Al,La,Mg)_2(Al,La,Mg)_1$ Pearson symbol: cF24, Prototype: Cu_2Mg, space group: $Fd\bar{3}m$	
$G^0_{Al:Al} = 43950$	[16]
$G^0_{La:La} = 53790$	
$G^0_{La:Al} = 119970$	
$G^0_{Al:La} = -150000 + 11.619T$	
$G^0_{Mg:La} = -26814.7 - 10.1377T$	[17]
$G^0_{Mg:Mg} = 15000$	[13]
$G^0_{Mg:Al} = 104970.96 - 16.46448T$	
$G^0_{Al:Mg} = 30000 + 4T$	
${}^0L_{Mg:Al,Mg} = {}^0L_{Al:Al,Mg} = 8000$	
${}^0L_{Mg,Al:Mg} = {}^0L_{Mg,Al:Al} = 15000$	
$G^0_{La:Mg} = 15000$	Present work
${}^0L_{La,Mg:La} = {}^0L_{Mg:La,Mg} = 130042$	
${}^0L_{Al,Mg:La} = -40095 + 25T$	
${}^1L_{Al,Mg:La} = 44422 - 14T$	
${}^2L_{Al,Mg:La} = -63171 + 27T$	
Phase: BCC_B2, Sublattice model: $(Al,La,Mg)_1(Al,La,Mg)_1$ Pearson symbol: cP2, Prototype: CsCl, space group: $Pm\bar{3}m$	
$G^0_{La:Mg} = G^0_{Mg:La} = -33402.3 + 9.188T$	[17]
$G^0_{Mg:Mg} = 0$	[21]
$G^0_{Al:Al} = G^0_{La:La} = 0$	Present work
$G^0_{La:Al} = G^0_{Al:La} = -65000$	
${}^0L_{La,Mg:La} = {}^0L_{La:La,Mg} = -14088.089 + 31.798T$	
${}^0L_{La,Mg:La,Mg} = -31250$	
${}^1L_{La,Mg:La} = {}^1L_{La:Mg,La} = -31000 - 15T$	
${}^1L_{Mg:La,Mg} = {}^1L_{La,Mg:Mg} = 24500 + 25T$	
${}^0L_{La:Al,Mg} = -75530 + 20T$	
Phase: τ, sublattice model: $(Al)_2(Mg)_{0.85}(La)_{0.15}$ crystallography is unknown	
$\Delta_f G^0 = -37412.3 + 5T$	Present work

action parameters. The characteristics of the invariant equilibria as well as shapes and locations of phase boundaries calculated with the new models are virtually indistinguishable from those in [17]. The kinks on the concentration dependencies of the molar Gibbs energies clearly seen in Figs. 1 and 2 are not suspicious, because their presence is typical when order/disorder transitions are handled using a two-sublattice model [22].

3. Optimization of the Al–La–Mg system

3.1. Literature data

Experimental investigations of the Al–La–Mg system published prior to 1988 were reviewed by Rogl [23]. They include an examination of the Al-rich liquidus surface [24], a partial 673 K isotherm in the 0–33 at.% La range [25], and a complete 673 K isothermal section [26]. Zheng et al. [24] studied the liquidus surface near the Al-rich corner of the Al–La–Mg system using X-ray diffraction (XRD) analysis, differential thermal analysis (DTA) and metallography, and found that temperature of the eutectic reaction $L \rightarrow \alpha\text{-}La_3Al_{11} + Al_3Mg_2 + Al$ was equal to 718 K.

Odinaev et al. [26] constructed the isothermal 673 K section using the XRD analysis of 115 annealed ternary alloys. Three phases containing all components were discovered, and the following stoichiometric formulae were assigned to them: $LaMg_{1-x}Al_x$, $LaMg_{2-x}Al_x$, and $Al_2Mg_{0.85}La_{0.15}$. Among those phases, only $La_{0.15}Mg_{0.85}Al_2$ was a truly ternary phase in the sense that it did not touch the sides of the Gibbs–Roseboom triangle. In the present work, this phase is named τ and treated as a stoichiometric compound; a lack of structural information does not allow suggesting a crystallographically better model for the τ phase. $LaMg_{1-x}Al_x$ has the B2 structure and is an extension of the binary LaMg phase capable of accommodating aluminum, whose solubility at 673 K reaches 20 at.%. $LaMg_{2-x}Al_x$ is the Laves_C15 phase whose homogeneity range at 673 K is interrupted by a miscibility gap.

A graphical representation of the experimental findings in [26] is not free from shortcomings. Firstly, the authors overlooked that $LaMg_{12}$ and $Al_{30}Mg_{23}$ were stable at 673 K and did not incorporate them into the isothermal section. Secondly, the homogeneity range of Laves_C15 sketched by Odinaev et al. [26] included $LaMg_2$ as a terminal point, although this binary compound was not stable 673 K. These two inconsistencies should not be forgotten when data for feeding an optimization procedure are decided upon, and when a calculated isothermal section is compared with that depicted in [26] in Section 3.4.

A continuing interest of Odinaev and his collaborators in the Al–Mg–R systems resulted in valuable experimental studies of the Al–Mg–Sc [27], Al–Mg–La [28], Al–Mg–Ce [29], Al–Mg–Nd [30], and Al–Mg–Pr [31] systems. In all cases, optical metallography, XRD analysis and DTA were utilized for building isoplethal and isothermal sections. In the case of the Al–Mg–La system, an examination of 134 alloys with compositions belonging to the Al–Mg–Al_2La subtriangle yielded seven vertical sections (which were all treated by Odinaev and Ganiev as pseudobinary without a convincing justification), liquidus temperatures and characteristics of six invariant reactions. The existence of the τ phase claimed in [26] was confirmed, and it was determined that $La_{0.15}Mg_{0.85}Al_2$ melted congruently at 828 K.

It seems reasonable to use all information from [28] in the course of thermodynamic optimization of the Al–La–Mg system, but there is a circumstance refraining one from doing so. The Al–Mg–Sc and Al–Mg–Ce systems, *i.e.*, the systems experimentally studied in [27,29], were optimized by Gröbner et al. [32,33]. In the latter two publications, it was convincingly shown that the isoplethal sections suggested by Odinaev could not be treated as pseudobinary. Also, calculated liquidus temperatures were surprisingly higher than the experimental values; for some compositions, a discrepancy exceeded three hundred degrees. A meticulous calorimetric investigation carried out by Gröbner et al. [33] resulted in liquidus temperatures conforming to the computed quantities. It is almost certain that the liquidus temperatures reported in [27,29] were burdened with an unknown systematic error. Since the same experimental technique was used for investigating Al–Mg–La system, it

Table 2
Chemical compositions of alloys used in the DTA (in wt.%).

Alloy name	Al		La		Mg	
	As weighed	Actual	As weighed	Actual	As weighed	Actual
Al60	60.00 ± 0.05	61.3 ± 0.1	20.10 ± 0.05	18.7 ± 0.1	19.90 ± 0.05	20.0 ± 0.1
Al70	70.00 ± 0.05	70.6 ± 0.1	15.07 ± 0.05	14.0 ± 0.1	14.93 ± 0.05	15.4 ± 0.1

was decided not to provide the optimization procedure with data on liquidus from [28], but to carry out a calorimetric investigation to judge whether they can be employed for this purpose.

3.2. Calorimetric study of Al–Mg–La alloys

A Netzsch STA 409 differential scanning calorimeter with power compensation was used to capture thermal events accompanying solidification of two alloys whose compositions are given in Table 2. Weighed amounts of Al (0.001 wt.% of impurities), La (0.1) and Mg (0.01) were placed in a graphite crucible and melted in an induction heating furnace under a protective dynamic Ar atmosphere. The melt was vigorously stirred with a boron nitride rod for several minutes to ensure its homogeneity. For each ingot, several small pieces were cut from different locations. The compositions of the specimens measured using the Inductively Coupled Plasma analysis were statistically indistinguishable, which suggested a macroscopic uniformity of the ingots.

Approximately 100 mg of each alloy were put in a stainless steel crucible, which then was sealed under Ar; a protective Ar atmosphere was also used during a calorimetric run. Since the samples were not annealed, only cooling curves were recorded. The Al60 alloy was examined within the 1223–573 K interval; for the Al70 alloy the range was 1123–573 K. By carrying out three runs for each alloy, a reproducibility of measurements was ensured.

Stainless steel crucibles are used in this investigation since it is known that the rate of dissolution of Fe in Al alloys is very low. Moreover, the passive film of chromium oxide formed on the surface of the steel inhibits an interaction between the alloy and the bulk of the crucible. Nevertheless, the Al–Mg–R alloys are very reactive in liquid state. Even inert metals such as Ta and Mo are reported to be attacked by these alloys [32]. To ensure that samples are not contaminated during the DTA experiment the exposure time is shortened by employing a rather high cooling rate of 10 K/min. Furthermore, fresh samples and new crucibles are used for each of the three runs.

Fig. 3 exemplifies typical cooling curves. Temperature associated with an exothermic event is defined as temperature at which the curve starts deviating from the baseline.

A shape and intensity of the peak observed at 719 K for both alloys point to an invariant reaction. As shown in Section 3.4, the peak at 794 K registered for the Al70 alloy may correspond to the start of FCC precipitation. The peaks at 1119 K and 1053 K correspond to the liquidus temperatures. Although it is usually deemed that peaks associated with the onset of solidification are quite pronounced, it is not the case for alloys with wide solidification ranges. For both Al60 and Al70 alloys, the liquidus temperatures determined in this work are dramatically higher than those given in [28].

It is worth mentioning that no microstructural characterization is performed on the prepared alloys. This is because, as stated before, the sole motive for the calorimetric investigation is to verify the reliability of the reported liquidus data. A phase identification of the samples could not provide further arguments for this purpose.

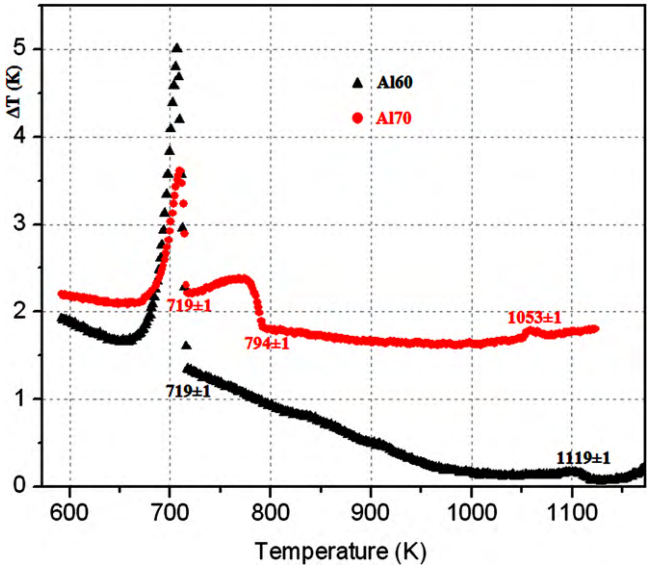

Fig. 3. DTA responses of the Al60 and Al70 alloy samples. The curve for the Al60 alloy is moved down 1 K for clarity.

3.3. Optimization: technicalities and outcome

The Redlich–Kister formalism was used to describe the excess Gibbs energy of the liquid phase in the Al–Mg [12] and La–Mg [17] systems. The thermodynamic properties of the liquid phase in the Al–La system were represented using an association model with Al, La and Al_2La sagaciously chosen as species [16]. The Muggianu method [34] was used to evaluate the excess Gibbs energy of the ternary liquid phase from the boundary binary systems. Interaction energy between Mg and Al_2La was not considered as an adjustable parameter and was set equal to zero.

The assessment was carried out using PARROT [20], the optimization module of Thermo-Calc [35]. Critically evaluated experimental information from [26,28] was used as input data for PARROT. Due to the arguments presented above, liquidus temperatures from [28] were not made use of. Such an omission meant that the assessment would in fact be based on low-temperature measurements carried out in the vicinity of 673 K. In order to get evidence that the thermodynamic model of the Al–La–Mg system remains reasonable at higher temperatures, the liquidus temperatures of Al60 and Al70 alloys were not passed to PARROT. Instead, their proximity to calculated liquidus temperatures was used as a semi-quantitative indication that the numerical values given in Table 1 would not yield absurd results at high temperatures contains information in a format suggested by the compound energy formalism [36]. To elaborate, let us consider a phase whose two-sublattice model is given by (1):

$$(Al_{y'_{Al}}, La_{y'_{La}}, Mg_{y'_{Mg}})_p (Al_{y''_{Al}}, La_{y''_{La}}, Mg_{y''_{Mg}})_q \quad (1)$$

where p and q are the numbers of sites; y'_i and y''_i are the site fractions of the constituent i on the first and second sublattices, correspondingly.

The expression for the Gibbs energy of formation per one formula unit of the phase from the components taken in their standard element reference (SER) states is written as follows:

$$\begin{aligned} G = {} & \sum_i \sum_j y'_i y''_j (G^{\circ}_{i:j} - pG^{ESR}_i - qG^{ESR}_j) \\ & + RT\left(p\sum_i y'_i \ln y'_i + q\sum_i y''_i \ln y''_i\right) \\ & + \sum_k y''_k \sum_i \sum_{j\neq i} y'_i y'_j \sum_{v=0} {}^{v}L_{i,j:k}(y'_i - y'_j)^v \\ & + \sum_k y'_k \sum_i \sum_{j\neq i} y''_i y''_j \sum_{v=0} {}^{v}L_{k:i,j}(y''_i - y''_j)^v \end{aligned} \quad (2)$$

where i,j, and k span over all the three elements. In this expression, $G^{\circ}_{i:j}$ is the Gibbs energy of the end-member $(i)_p(j)_q$, and ${}^{v}L$ are interaction parameters. The data for G^{ESR}_i are taken

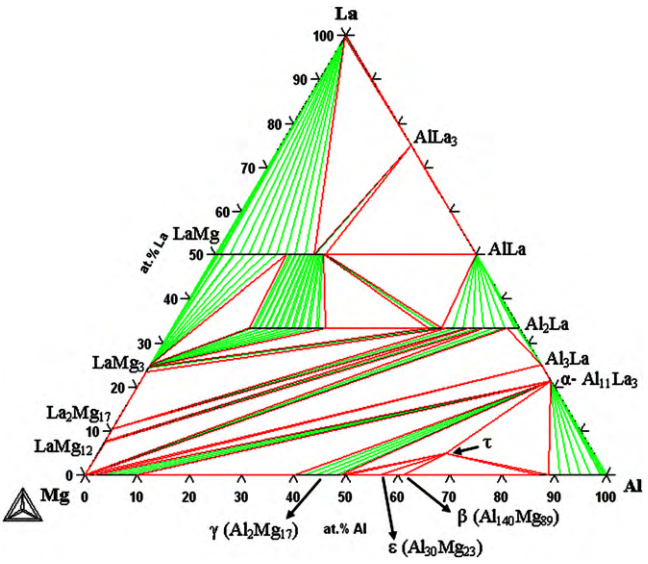

Fig. 4. Calculated 673 K isothermal section.

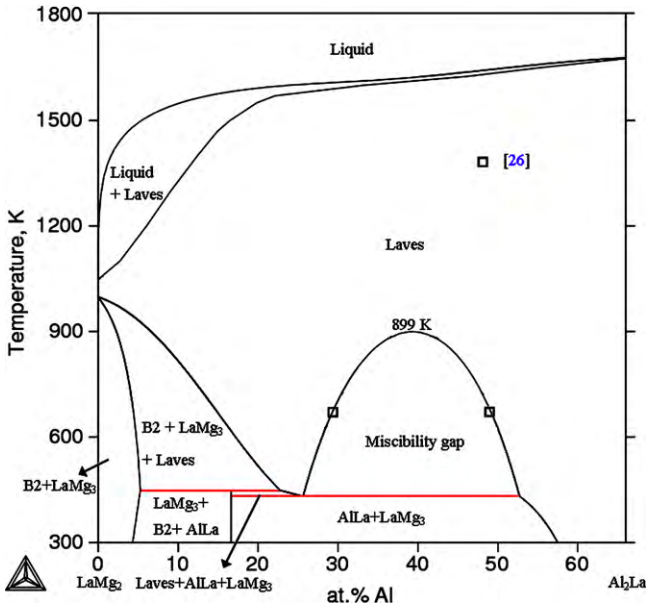

Fig. 6. $LaMg_2$–$LaAl_2$ isoplethal section.

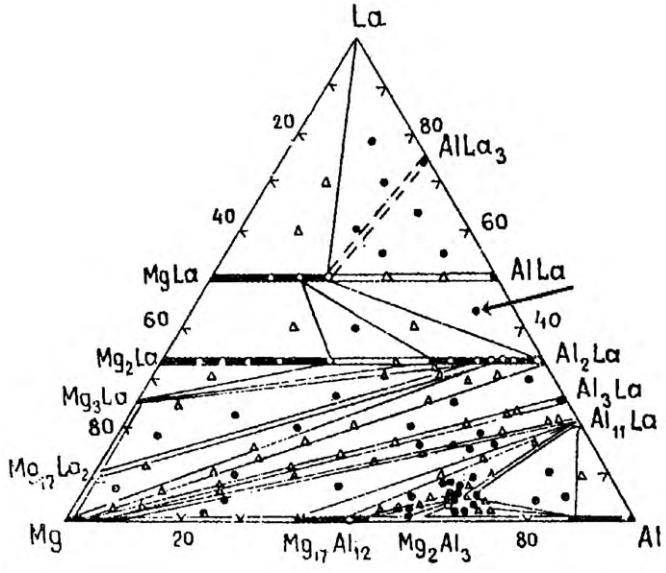

Fig. 5. Experimentally established 673 K isothermal section [26] (○, △ and ● represent one-, two- and three-phase states).

from [37]. It should be noted that the last two terms of (2) represent the simplest form of the excess Gibbs energy. A detailed explanation on how to apply compound energy formalism to the B2–A2 order–disorder transformation can be found in [19].

3.4. Calculations vs. experiment

At first glance, there are non-negligible dissimilarities between the calculated and experimental sections shown in Figs. 4 and 5. In fact, however, an agreement is good if the following is kept in mind. Firstly, the binary $LaMg_2$ phase is unstable at 673 K, which means that the homogeneity range of the ternary Laves_C15 phase cannot touch the La–Mg side of the Gibbs–Roseboom triangle at this temperature. Secondly, the existence of $LaMg_{12}$ and $Al_{30}Mg_{23}$, which was overlooked in [26], results in phase boundaries not seen in Fig. 5. Thirdly, an interpretation of the microstructures of annealed alloys led Odinaev et al. to a conclusion that at 673 K, a two-phase equilibrium between Al_2La and AlLa was possible only in the binary Al–La system. However, if Al_2La dissolved Mg, then it would be possible for this two-phase equilibrium to extend into the ternary region. This scenario is predicted in the calculated isotherm. It should be noticed that the conclusion of [26] hinges on the experimental point marked with the arrow in Fig. 5, and that it is situated very close to the calculated boundary between the two- and three-phase fields. In other words, although the two isothermal sections are topologically different, the position of the arrowed data point contradicts none of them.

It is apparent from Fig. 4 that there is a range of concentrations within which Laves_C15 is internally unstable. A miscibility gap associated with this instability is shown in Fig. 6. The presence of a miscibility gap is not an unusual phenomenon for ternary Laves phases [38]. The closest resemblance to Fig. 6 can be found in the Al–Ce–Mg and Al–Mg–Nd systems where miscibility gaps are experimentally observed for the $(Al,Mg)_2Ce$ and $(Al,Mg)_2Nd$ Laves phases [39,40].

As mentioned above, only critically evaluated data from [28] were used in the course of optimization. In particular, only experimental points on the vertical sections allowing an unquestionably correct interpretation were employed. From this angle, it is not surprising that the calculated isopleths perceptually deviate from those drawn by Odinaev and Ganiev. An instructive example is given in Fig. 7. Shockingly low liquidus temperatures in [28] are exactly the same phenomenon encountered by Gröbner et al. for the Al–Mg–Sc [32], Al–Mg–Ce [33] and Al–Mg–Gd [41] systems. The liquidus temperatures calorimetrically determined in this work for the Al60 and Al70 alloys match well with the model's prediction. It is worth accentuating that a decent agreement was obtained without introducing ternary interaction parameters in the model adopted for the liquid phase.

It should be reiterated that the vertical sections in [28] were construed as pseudobinary without presenting a convincing proof. The presence of the α-La_3Al_{11} phase, however, is incompatible with that postulate.

The most striking feature of the calculated liquidus surface whose projection is shown in Fig. 8 is a prominent high-temperature hill within the region of primary solidification of the Laves_C15 phase. It is shaped and positioned in such a manner, that the La and Al corners become separated. An implication of this fea-

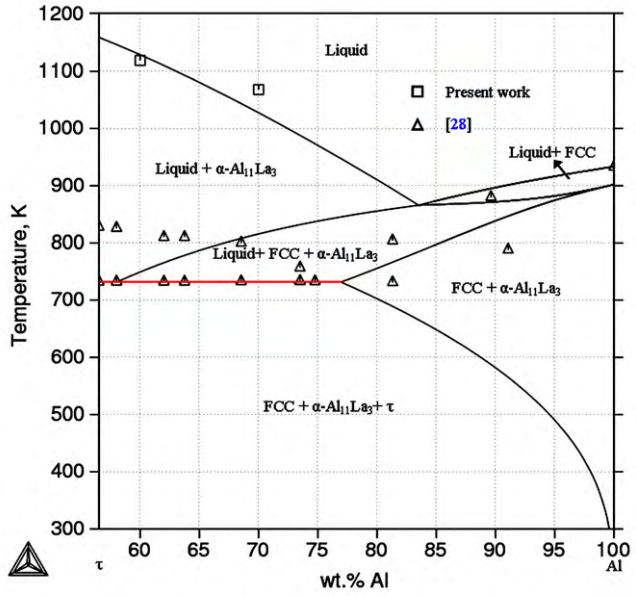

Fig. 7. Experimental points superposed on the calculated Al–τ isopleth.

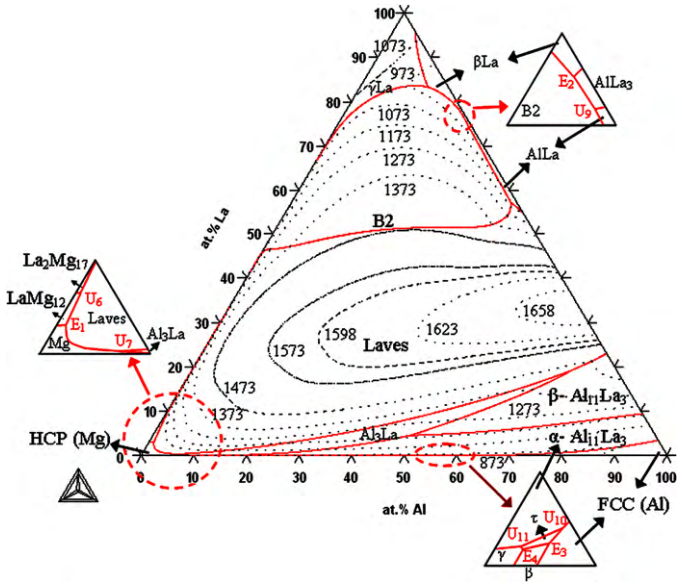

Fig. 8. Projection of the liquidus surface and primary solidification fields (temperatures are in Kelvin).

ture on the manufacturability of Al/RM composites is discussed in the next section.

Characteristics of all invariant reactions in the Al–La–Mg system can be found in Appendix A. Where applicable, the calculated

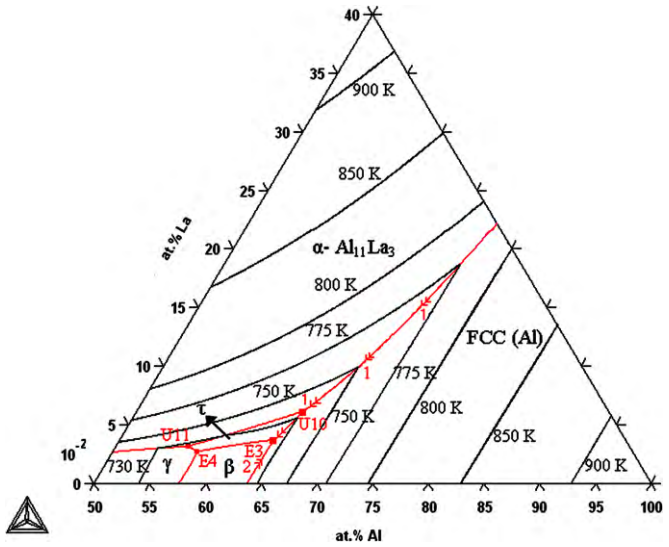

Fig. 9. Primary solidification region of the FCC phase.

temperatures and mole fractions of aluminum and lanthanum in the liquid phase are compared with corresponding experimental values published in [28]. If it is assumed that the Scheil mode of solidification is operative, then the thermal event detected at 718 K in both Al60 and Al70 alloys can confidently be identified with the eutectic reaction $L \rightarrow Al + \tau + \beta$. The calculated solidification path of Scheil for the Al70 alloy shows a $L \rightarrow \alpha\text{-}Al_{11}La_3 + Al$ reaction to happen at 815 K. This is relatively close to the peak at 794 K seen in the DTA response of the Al70 alloy. It is worth noting that this is a monovariant eutectic reaction whose temperature critically depends on the composition of the remaining melt. It is calculated that a 20 K decrease in the temperature of this reaction can be caused by only 1 wt.% decrease in the concentration of La. This may explain the difference between the results of calculation and experiment.

3.5. Two-phase Al/RM material

Let us recall that there was a pragmatic motivation this work originated from. It was intended to estimate a possibility to produce a material containing a ductile FCC matrix with inclusions of ductile RM intermetallics *via* casting. The thermodynamic model of the Al–La–Mg system presented here leads to a definite conclusion that the possibility does not exist.

Let us arrive at this verdict by assuming that the solidification proceeds according to the Scheil–Gulliver paradigm [42,43]. This is a practical assumption since a rather slow cooling rate achieved in commercial direct-chill casting of Al alloys satisfies the conditions of the Scheil–Gulliver method. Now let us inspect Figs. 9 and 10 and realize that two solidification trajectories are possible for alloys whose overall compositions belong to the FCC primary crystalliza-

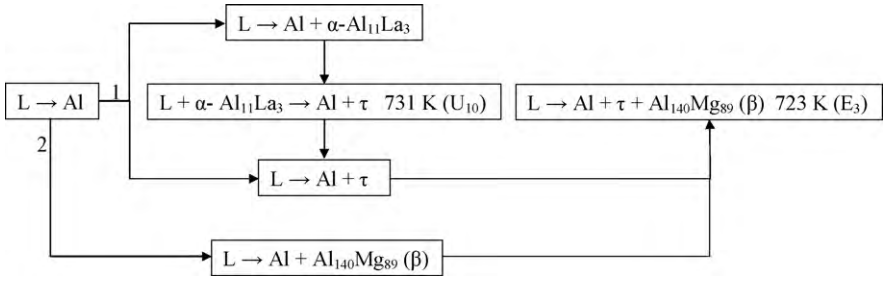

Fig. 10. Two kinds of solidification paths of an alloy with a net composition falling into the region of primary solidification of the FCC phase.

tion field. Apparently, none of these paths results in the formation of the B2 phase.

The analysis can be extended by making a technologically questionable assumption that the net composition of an alloy is outside the FCC primary crystallization domain. In principle, it is possible that both the B2 and FCC phases will form during casting, but in order to make the desired material; they must not merely form from a solidifying melt, but coprecipitate from it. The coprecipitation of the two phases depends on the existence of a boundary between primary solidification regions of them in the form of a temperature valley (*i.e.* a monovariant eutectic reaction L → FCC + B2). In the case of the Al–La–Mg system however, such a boundary does not exist primarily because the high-temperature hill of primary solidification of the Laves phase has completely separated the primary solidification domains of the B2 and FCC phases.

Similarities between properties of various R metals suggest that fabrication of a two-phase material containing other RMg compounds may be hindered by the same phenomenon. In fact an examination of calculated liquidus surfaces of other optimized Al–Mg–R systems [32,33,39,44–46] proves that the in all cases the primary regions of Al-rich FCC and B2 phases do not intersect, and hence, the Al/RMg composite cannot form during solidification.

4. Conclusions

Motivated by the needs of the automotive industry and inspired by the discovery of a family of ductile intermetallics, fabrication of an Al/LaMg two-phase material by casting was objectified. To answer the question "Whether ductile LaMg phase forms during solidification?" one can rely upon predictions of Scheil–Gulliver method. Such an analysis requires the availability of a thermodynamic database on Al–La–Mg ternary system. To develop a self-consistent database, it deemed necessary to modify the descriptions of the Laves and B2 intermetallic phases in the La–Mg binary sub-system. These modifications were incorporated by a partial re-optimized of the La–Mg system. Hinted by the experimental investigations on other Al–Mg–R systems, DTA experiments were performed on two Al-rich alloys. The results revealed that the ternary liquidus temperatures are considerably higher than those presented in the literature. The Al–La–Mg ternary system was optimized using the PARROT module of the Thermo-Calc software. A reasonable agreement between calculated data and experimental results warranted a utilization of the developed database for various thermodynamic calculations including Scheil–Gulliver solidification paths. The predicted paths show that the coprecipitation of the FCC and B2 phases needed for the fabrication of the desired two-phase material is impossible. This unfavorable situation is caused by the presence of a high-temperature crystallization region of the Laves phase.

Acknowledgements

The authors gratefully acknowledge the financial support of the Auto 21 Research Initiative. The in-kind support from Novelis is greatly appreciated.

Appendix A.

The table below contains characteristics of all invariant reactions in the Al–La–Mg system. *c* in *c*/*e* in the last 5 rows is a *c*omputed quantity, and *e* is a corresponding *e*xperimental value from [28].

Reaction	Type [47]	T (K)	at.% in liquid	
			Al	La
$L + Al_7La_3 \rightarrow \beta\text{-}Al_{11}La_3 + Laves$	U_1	1483	75.5	21.8
$L \rightarrow B2 + Laves$	Max	1466	24	48
$L + \beta\text{-}Al_{11}La_3 \rightarrow Laves + Al_3La$	U_2	1438	72.6	19.5
$L \rightarrow \beta\text{-}Al_{11}La_3 + \alpha\text{-}Al_{11}La_3 + Al_3La$	D_1	1188	49	4.5
$L + Laves \rightarrow B2 + AlLa$	U_3	1127	42	57
$L \rightarrow LaMg_3 + Laves$	Max	1071.5	0.004	24.7
$L \rightarrow B2 + \gamma La$	Max	1028	1.7	78
$L + LaMg_3 \rightarrow La_2Mg_{17} + Laves$	U_4	944.5	0.13	10
$L + \gamma La \rightarrow B2 + \beta La$	U_5	922	12.5	83.8
$L + La_2Mg_{17} \rightarrow LaMg_{12} + Laves$	U_6	920	0.5	6.5
$L \rightarrow Mg + Laves$	Max	899.5	2.6	1
$L + Laves \rightarrow Al_3La + Mg$	U_7	885	6.6	0.3
$L \rightarrow LaMg_{12} + Mg + Laves$	E_1	881	0.86	3.1
$L + Al_3La \rightarrow Mg + \alpha\text{-}Al_{11}La_3$	U_8	826.5	16.4	0.07
$L + AlLa \rightarrow B2 + AlLa_3$	U_9	794.5	22.5	77.2
$L \rightarrow B2 + \beta La + AlLa_3$	E_2	792	21.2	78.5
$L \rightarrow \gamma + \alpha\text{-}Al_{11}La_3$	Max	736.5	46.3	0.02
$L \rightarrow \tau + \alpha\text{-}Al_{11}La_3$	Max	732	62.3	0.05
$L \rightarrow \tau + \beta$	Max	725	61.2	0.03
$L + \alpha\text{-}Al_{11}La_3 \rightarrow Al + \tau$	U_{10}	731/732	65/81	0.06/2.8
$L + \alpha\text{-}Al_{11}La_3 \rightarrow \gamma + \tau$	U_{11}	725/707	56.4/49.1	0.03/2.9
$L \rightarrow Al + \tau + \beta$	E_3	723/706/719 [this work]	63.8/63	0.04/1.1
$L \rightarrow \gamma + \tau + \beta$	E_4	722.4/709	57.6/55.5	0.03/0.9
$L \rightarrow \gamma + Mg + \alpha\text{-}Al_{11}La_3$	E_5	709/705	31/30.2	0.008/2.8

References

[1] K.A. Gschneidner Jr., A.M. Russell, A.O. Pecharsky, J.R. Morris, Z. Zhang, T.A. Lograsso, D. Hsu, C.H.C. Lo, Y. Ye, A. Slager, Nat. Mater. 2 (9) (2003) 587–590.
[2] A.M. Russell, Z. Zhang, T.A. Lograsso, C.C.H. Lo, A.O. Pecharsky, J.R. Morris, Y. Ye, K.A. Gschneidner Jr., A.J. Slager, Acta Mater. 52 (13) (2004) 4033–4040.
[3] J.R. Morris, Y. Ye, Y. Lee, B.N. Harmon, K.A. Gschneidner Jr., A.M. Russell, Acta Mater. 52 (16) (2004) 4849–4857.
[4] A.M. Russell, Z. Zhang, K.A. Gschneidner Jr., T.A. Lograsso, A.O. Pecharsky, A.J. Slager, D.C. Kesse, Intermetallics 13 (6) (2005) 565–571.
[5] Z. Zhang, A.M. Russell, S.B. Biner, K.A. Gschneidner Jr., C.C.H. Lo, Intermetallics 13 (5) (2005) 559–564.
[6] S. Xie, K.A. Gschneidner Jr., A.M. Russell, Scr. Mater. 59 (8) (2008) 810–813.
[7] J.A. Wollmershauser, S. Kabra, S.R. Agnew, Acta Mater. 57 (1) (2009) 213–223.
[8] C.W. Sinclair, J.D. Embury, G.C. Weatherly, Mater. Sci. Eng. A A272 (1) (1999) 90–98.
[9] A.M. Russell, L.S. Chumbley, Y. Tian, Adv. Eng. Mater. 2 (1–2) (2000) 11–22.
[10] W.A. Spitzig, P.D. Krotz, Acta Metall. 36 (7) (1988) 1709–1715.
[11] H.L. Lukas, S.G. Fries, B. Sundman, Computational Thermodynamics: The Calphad Method, 1st ed., Cambridge University Press, New York, 2007.
[12] P. Liang, H.L. Su, P. Donnadieu, M.G. Harmelin, A. Quivy, P. Ochin, G. Effenberg, H.J. Seifert, H.L. Lukas, F. Aldinger, Z. Metallkd. 89 (8) (1998) 536–540.
[13] N. Saunders, CALPHAD: Comput. Coupling Phase Diagrams Thermochem. 14 (1) (1990) 61–70.
[14] F. Yin, X. Su, Z. Li, M. Huang, Y. Shi, J. Alloys Compd. 302 (1–2) (2000) 169–172.
[15] G. Cacciamani, R. Ferro, CALPHAD: Comput. Coupling Phase Diagrams Thermochem. 25 (4) (2001) 583–597.
[16] S.H. Zhou, R.E. Napolitano, Acta Mater. 54 (3) (2006) 831–840.
[17] C. Guo, Z. Du, J. Alloys Compd. 385 (1–2) (2004) 109–113.
[18] I. Ansara, T.G. Chart, A. Guillermet Fernández, F.H. Hayes, U.R. Kattner, D.G. Pettifor, N. Saunders, K. Zeng, CALPHAD: Comput. Coupling Phase Diagrams Thermochem. 21 (2) (1997) 171–218.
[19] N. Duppin, I. Ansara, Z. Metallkd. 90 (1) (1999) 76–85.
[20] B. Jansson, Evaluation of Parameters in Thermochemical Models Using Different Types of Experimental Data Simultaneously, TRITA-MAC-0234, Royal Institute of Technology, Sweden, 1984.
[21] O.B. Fabrichnaya, H.L. Lukas, G. Effenberg, F. Aldinger, Intermetallics 11 (11–12) (2003) 1183–1188.
[22] W.A. Oates, F. Zhang, S.-L. Chen, Y.A. Chang, CALPHAD: Comput. Coupling Phase Diagrams Thermochem. 23 (2) (1999) 181–188.
[23] P. Rogl, in: G. Petzow, G. Effenberg (Eds.), Ternary Alloys: A Comprehensive Compendium of Evaluated Constitutional Data and Phase Diagrams, Weinheim, New York, 1988.
[24] C. Zheng, Y. Xing, J. Qian, Y. Ye, Acta Metall. Sin. 19 (6) (1983) 515–520.
[25] O.S. Zarechnyuk, V.V. Kinzhibalo, A.T. Tyvanchuk, R.M. Rykhal, Russ. Metall. 5 (1981) 173–175.
[26] Kh.O. Odinaev, I.N. Ganiev, V.V. Kinzhibalo, A.T. Tyvanchuk, Izv. Vyssh. Uchebn. Zaved., Tsvetn. Metall. 2 (1988) 81–85.
[27] Kh.O. Odinaev, I.N. Ganiev, A.V. Vakhobov, Russ. Metall. 4 (1991) 200–203.
[28] Kh.O. Odinaev, I.N. Ganiev, Russ. Metall. 2 (1995) 146–150.
[29] Kh.O. Odinaev, I.N. Ganiev, A.Z. Ikromov, Russ. Metall. 3 (1996) 122–125.

[30] Kh.O. Odinaev, I.N. Ganiev, A.Z. Ikromov, Russ. Metall. 4 (1996) 153–156.
[31] Kh.O. Odinaev, I.N. Ganiev, A.Z. Ikromov, Russ. Metall. 3 (1996) 126–129.
[32] J. Grobner, R. Schmid-Fetzer, A. Pisch, G. Cacciamani, P. Riani, N. Parodi, G. Borzone, A. Saccone, R. Ferro, Z. Metallkd. 90 (11) (1999) 872–880.
[33] J. Grobner, D. Kevorkov, R. Schmid-Fetzer, Intermetallics 10 (5) (2002) 415–422.
[34] Y.M. Muggianu, M. Gambino, J.P. Bros, J. Chem. Phys. 72 (1) (1975) 83–88.
[35] J.-O. Anderson, T. Helander, L. Höglund, P. Shi, B. Sundman, CALPHAD: Comput. Coupling Phase Diagrams Thermochem. 26 (2) (2002) 273–312.
[36] M. Hillert, J. Alloys Compd. 320 (2001) 161–176.
[37] A.T. Dinsdale, PHAD: Comput. Coupling Phase Diagrams Thermochem. 15 (4) (1991) 317–425.
[38] F. Stein, M. Palm, G. Sauthoff, Intermetallics 13 (10) (2005) 1056–1074.
[39] Kh.O. Odinaev, I.N. Ganiev, V.V. Kinzhibalo, Kh.K. Kurbanov, Izv. Vyssh. Uchebn. Zaved., Tsvetn. Metall. 4 (1989) 75–77.
[40] Kh.O. Odinaev, I.N. Ganiev, V.V. Kinzhibalo, A.T. Tyvanchuk, Izv. Vyssh. Uchebn. Zaved., Tsvetn. Metall. 4 (1988) 94–97.
[41] J. Grobner, D. Kevorkov, R. Schmid-Fetzer, Z. Metallkd. 92 (1) (2001) 22–27.
[42] G.H. Gulliver, J. Inst. Met. 9 (1913) 120–157.
[43] E. Scheil, Z. Metallkd. 34 (1942) 70–72.
[44] G. Cacciamani, A. Saccone, S. De Negri, R. Ferro, J. Phase Equilibr. 23 (1) (2002) 38–50.
[45] G. Cacciamani, S. De Negri, A. Saccone, R. Ferro, Intermetallics 11 (11–12) (2003) 1135–1151.
[46] S. Al Shakhshir, M. Medraj, J. Phase Equilibr. Diffus. 27 (3) (2006) 231–244.
[47] H.L. Lukas, E.T. Henig, G. Petzow, Z. Metallkd. 77 (6) (1986) 360–367.